# Amphipol-facilitated elucidation of the functional tetrameric complex of full-length cytochrome P450 CYP2B4 and NADPH-cytochrome P450 oxidoreductase

Received for publication, February 22, 2021, and in revised form, April 4, 2021 Published, Papers in Press, April 9, 2021,
https://doi.org/10.1016/j.jbc.2021.100645

**Shen Cheng**[‡], **Zhiyuan Bo**[‡], **Paul Hollenberg, Yoichi Osawa, and Haoming Zhang**[*]
*From the Department of Pharmacology, The University of Michigan Medical School, Ann Arbor, Michigan, USA*

Edited by F. Peter Guengerich

**Interactions of membrane-bound mammalian cytochromes P450 (CYPs) with NADPH-cytochrome P450 oxidoreductase (POR), which are required for metabolism of xenobiotics, are facilitated by membrane lipids. A variety of membrane mimetics, such as phospholipid liposomes and nanodiscs, have been used to simulate the membrane to form catalytically active CYP:POR complexes. However, the exact mechanism(s) of these interactions are unclear because of the absence of structural information of full-length mammalian CYP:POR complexes in membranes. Herein, we report the use of amphipols (APols) to form a fully functional, soluble, homogeneous preparation of full-length CYP:POR complexes amenable to biochemical and structural study. Incorporation of CYP2B4 and POR into APols resulted in a CYP2B4:POR complex with a stoichiometry of 1:1, which was fully functional in demethylating benzphetamine at a turnover rate of 37.7 ± 2.2 $min^{-1}$, with a coupling efficiency of 40%. Interestingly, the stable complex had a molecular weight ($M_w$) of 338 ± 22 kDa determined by multiangle light scattering, suggestive of a tetrameric complex of 2CYP2B4:2POR embedded in one APol nanoparticle. Moreover, negative stain electron microscopy (EM) validated the homogeneity of the complex and allowed us to generate a three-dimensional EM map and model consistent with the tetramer observed in solution. This first report of the full-length mammalian CYP:POR complex by transmission EM not only reveals the architecture that facilitates electron transfer but also highlights a potential use of APols in biochemical and structural studies of functional CYP complexes with redox partners.**

Mammalian cytochromes P450 (CYPs or P450s) are a superfamily of hemoproteins that play critical roles in the oxidative metabolism of xenobiotics (drugs or toxins) and the biosynthesis of endobiotics (sterols or fatty acids) (1). Oxidative metabolism and biosynthesis by P450s require the sequential transfer of two electrons from NADPH-cytochrome P450 oxidoreductase (POR). Therefore, the interactions of P450s with POR play critical roles in drug metabolism and steroidogenesis. The relative ratio of P450:POR in the ER membrane is estimated to be ∼20:1 (2, 3). It is intriguing how POR interacts with an excess of P450s to selectively transfer electrons required for drug metabolism while limiting production of reactive oxygen species. Nearly 60 years have elapsed since the discovery of P450s (4), and yet, we know little structurally about such vital interactions that dictate drug metabolism. This lack of understanding is due in large part to lack of experimental approaches to obtain 3D structures of mammalian P450:POR complexes.

Historically P450-catalyzed reactions were recapitulated in reconstituted phospholipid liposomes since the seminal work of Drs. Anthony Lu and Minor J. Coon (5). With both P450 and POR reconstituted in the phospholipid liposomes, various biochemical and biophysical approaches were applied and provided a wealth of information regarding the kinetics and mechanism of P450-catalyzed reactions. However, the reconstituted system is inherently heterogeneous and not amendable to structural analysis. Since then, more refined preparations were achieved by incorporation of P450 and POR in membrane mimetics of apolipoprotein A-1 or peptide-based nanodiscs (6–9). These preparations have presented the possibilities for biophysical studies of P450 and POR in phospholipid bilayers. Atomic force microscopy revealed the topology of CYP2B4 incorporated into apolipoprotein A-1 nanodiscs (10). A series of studies using solid state NMR revealed the interfaces of CYP2B4 with the FMN-binding domain of POR or cytochrome $b_5$ (cyt $b_5$), another redox partner of P450s, in peptide-based nanodiscs and reinforced the idea that the proximal side of CYP2B4 interacts with its redox partners (8, 9, 11). So far, no 3D structures of mammalian P450:POR complexes have been determined experimentally. Much of our current knowledge about the structure of the complex is derived from molecular dynamics simulations (12, 13).

An alternative approach to apolipoprotein A-1 or peptide-based nanodiscs is to incorporate full-length CYP2B4 and POR in amphipols (APols). APols are amphipathic polymers that self-assemble in aqueous solution to compact globular nanoparticles. Functioning like hydrophobic “sinks”, the APol nanoparticles tightly bind to the transmembrane regions of membrane proteins to prevent aggregation and stabilize

[‡] These authors contributed equally to this work.
[*] For correspondence: Haoming Zhang, haom@umich.edu.
Present address for Shen Cheng: Department of Experimental and Clinical Pharmacology, College of Pharmacy, University of Minnesota, Minneapolis, MN, USA.

membrane proteins in native states (14–16). Atomic structures of a number of membrane proteins have been determined with TEM once they are incorporated in APols (17, 18). Laursen *et al.* attempted to reconstitute plant CYP enzymes and POR into APol $A_{8-35}$ but failed to obtain a fully active complex of CYP:POR complex (19). In this work, we presented a novel preparation of a fully functional mammalian CYP2B4:POR complex in APols. The high homogeneity of the purified complex allowed us to reveal the architecture of a mammalian CYP:POR complex for the first time by negative stain electron microscopy (EM).

## Results

### *Preparations of the CYP2B4:POR complex in APols*

Incubation of full-length preparations of CYP2B4 and POR in the presence of APol $A_{8-35}$, free of detergents, led to co-elution of both proteins from Ni-NTA resin even though POR did not contain a His-tag, as shown in Figure 1*A* (Lane 6–8). Free POR was washed off the Ni-NTA resin (Lane 3–5, Fig. 1*A*). Co-elution of CYP2B4 and POR suggests incorporation of both proteins into APols. Approximately 60% of the total protein in the original incubation was recovered in the elution (Fig. 1*B*). As shown in Figure 1*C*, further purification by size-exclusion chromatography (SEC) exhibited a prominent peak at 9 ml and a shoulder at 7.8 ml. The corresponding $M_w$ values were estimated at 351 and 2441 kDa respectively based on calibration with protein standards (see Fig. S1). In comparison, the CYP2B4 and POR reconstituted in 1,2-dilauroyl-sn-glycero-3-phosphocholine (DLPC) liposomes eluted at 7.6 ml with an estimated $M_w$ of 3372 kDa, indicative of large oligomers. The complex in APols exhibited a typical ferrous carbon monoxide (CO) spectrum (Fig. 1*D*), indicative of an intact active site of CYP2B4. This is confirmed by determination of the catalytic activity as shown in Table 1. In APols, the turnover rates for NADPH consumption and norbenzphetamine production were determined to be 93.2 ± 0.14 and 37.7 ± 2.2 $min^{-1}$, respectively, which yielded a coupling efficiency of 40%. In the reconstituted system, the respective rates were 64.2 ± 0.14 and 30.1 ± 2.7 $min^{-1}$ with a couple efficiency of 47%, in agreement with previously reported values (20, 21). It is clear that the complex in APols is fully functional.

### *Stoichiometry and homogeneity of the CYP2B4:POR complex in APols*

The stoichiometry and homogeneity of the complex are two parameters critical for single particle analysis by TEM. Thus, both were determined as shown in Figure 2. The stoichiometry of the complex was determined with two methods, one based on protein content following separation by SDS-PAGE and the other on cofactor heme and flavin adenine dinucleotide (FAD) (see Fig. S2). Quantitation of the protein contents present in the complex gave a molar ratio of CYP2B4:POR of 1.2 ± 0.21, whereas quantitation of the heme of CYP2B4 and the FAD of POR gave a molar ratio of 1.1 ± 0.08. Both results suggest an approximately equal ratio of CYP2B4:POR. Presence of an equal ratio of CYP2B4 and POR in the complex is also consistent with the $M_w$ of the complex determined by SEC-multiangle light scattering (SEC-MALS) shown in Figure 2*B*. The average $M_w$ of the complex is 338 ± 22 kDa, which approximates the sum of 310 kDa from two CYP2B4 (114 kDa), two POR (156 kDa), and one APol nanoparticle of ~40 kDa (14). The SEC-MALS profile under the peak at 9 ml is

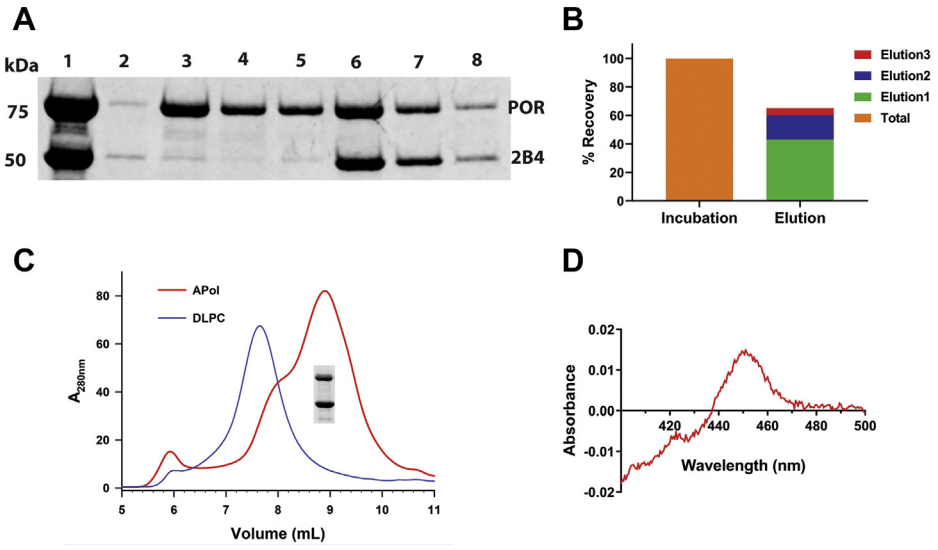


**Figure 1. Preparation of the CYP2B4:POR complex in APols**. Full-length CYP2B4 and POR (10 μM each) were incubated with APol $A_{8-35}$ overnight at pH 7.4. The incorporated complex was then purified using Ni-NTA resin and SEC before further use. *A*, SDS-PAGE of various fractions from purifications using Ni-NTA resin. Lanes 1 to 8 represent the initial incubation (Lane 1), unbound proteins (Lane 2), fractions from three consecutive washes with 10 mM imidazole (Lane 3–5), and the fractions from three consecutive elution with 0.3 M imidazole (Lane 6–8). *B*, percentage of the eluted protein (Lane 6–8 in *Panel A*) relative to the total protein (Lane 1 in *Panel A*). The percentage was quantified by gel densitometry. *C*, the protein eluted from the Ni-NTA resin was further purified by SEC (*red trace*), in comparison with the CYP2B4 and POR reconstituted in DLPC liposomes (*blue trace*). The two protein bands in the inset are POR and CYP2B4 at 75 and 50 kDa respectively. *D*, reduced CO spectrum for the peak fraction from the SEC purification shown in (*C*). APol, amphipol; DLPC, 1,2-dilauroyl-sn-glycero-3-phosphocholine; POR, NADPH-cytochrome P450 oxidoreductase.

**Table 1**
**Catalytic activities of the purified CYP2B4:POR complex in APol for N-demethylation of benzphetamine and NADPH oxidation**

| Preparations | NADPH oxidation ($min^{-1}$) | Product norBNZ ($min^{-1}$) | Coupling% |
|---|---|---|---|
| 2B4:POR in APol | 93.2 ± 0.14 | 37.7 ± 2.2 | 40 |
| 2B4:POR in DLPC | 64.2 ± 0.14 | 30.1 ± 2.7 | 47 |

APol, amphipol; DLPC, 1,2-dilauroyl-sn-glycero-3-phosphocholine; norBNZ, norbenzphetamine; POR, NADPH-cytochrome P450 oxidoreductase.
The activities were averaged over three different measurements and expressed as mean ± SD. Both rates were obtained in the presence of 1 mM benzphetamine as described in Experimental procedures.

homogenous as indicated by a horizontal red bar, even though the early elution before peaking showed slight heterogeneity as indicated by a slanted mass profile, indicative of the presence of other oligomers than the predominant tetramer.

### *Chemical crosslinking to stabilize the CYP2B4:POR complex in APols*

To examine whether the four units of the CYP2B4:POR complex in solution are closely associated with one another, we attempted to crosslink them with 1-ethyl-3-(3-dimethylaminopropyl)-carbodiimide (EDC). As shown in Figure 3*A*, the complex was completely crosslinked at ≥5 mM EDC leading to a high $M_w$ band. The high $M_w$ band contained both CYP2B4 and POR, indicative of the complex, and migrated at >460 kDa, as shown in Figure 3*B*. It is of note that crosslinked proteins may not migrate consistent with the $M_w$ because of a variety of factors such as charge, size, and shape of denatured proteins (22). In marked contrast, crosslinking of the reconstituted CYP2B4:POR complex in DLPC liposomes with EDC exhibited multiple bands, and the complex was not fully crosslinked even at 10 mM (see Fig. S3). These results suggest that the complex in APols is a relatively homogenous and tightly packed multiunit complex.

### *Single particle analysis of the CYP2B4:POR complex in APols by negative stain EM*

Initial imaging of negative stained micrographs of the CYP2B4:POR complex in APols showed a significant degree of heterogeneity likely because of dehydration in negative staining processes (see Fig. S4), which precluded further structural analysis. Because the complex in APols can be crosslinked by EDC, we thus utilized gradient fixation or GraFix, developed by Dr Stark's group, to further stabilize the complex by chemical crosslinking with glutaraldehyde before negative stain EM imaging (23). This was done to prevent dissociation of the multiunit complex resulting from dehydration, improve homogeneity, and minimize reconstruction artifacts.

The complex treated with GraFix exhibited greatly improved homogeneity in negative stain EM. As shown in Figure 4*A*, homogenous single particles of the complex were observed on a typical micrograph with a dimension of ∼150 Å. The single particles boxed in red show a clear view of four lobes of densities. The 2D class averages from reference-free alignment of 10,766 single particles are shown in Figure 4*B*. Those boxed in red show a clear projection of a tetrameric complex. The 2D class averages likely representing the tetramer allowed us to reconstruct a 3D EM map as shown in Figure 5. According to conventional Fourier shell correlation threshold criteria at 0.5, the 3D EM map displays a resolution of 27 Å (Fig. 5*A*). The top view of the 3D EM map shows four lobes of density (Fig. 5*B*), a pair of which are larger (∼77 Å) than the other two (∼54 Å). In contrast to the top view, the bottom view also shows EM density (Fig. 5*C*), which likely arises from the APol and N-termini of CYP2B4 and POR. The side view of the 3D EM map displays close association of a large bowl-shaped density with a small spherical density likely representing POR and CYP2B4 respectively, as shown in Figure 5*D*.

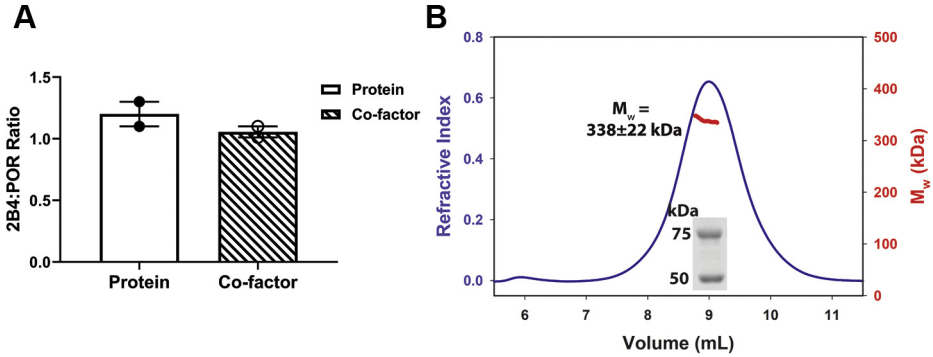


**Figure 2. Stoichiometry and homogeneity of the purified CYP2B4:POR complex in APols**. *A*, the stoichiometry of the purified CYP2B4:POR complex in APol determined by quantitation of protein and cofactors (heme of CYP2B4 and FAD of POR). *B*, homogeneity of the purified complex as determined by SEC-MALS. The *red bar* indicates $M_w$, and the SDS-PAGE gel indicates presence of both CYP2B4 and POR under the peak. The two protein bands in the inset are POR and CYP2B4 at 75 and 50 kDa, respectively. APol, amphipol; FAD, flavin adenine dinucleotide; POR, NADPH-cytochrome P450 oxidoreductase; SEC, size-exclusion chromatography; SEC-MALS, SEC-multiangle light scattering.

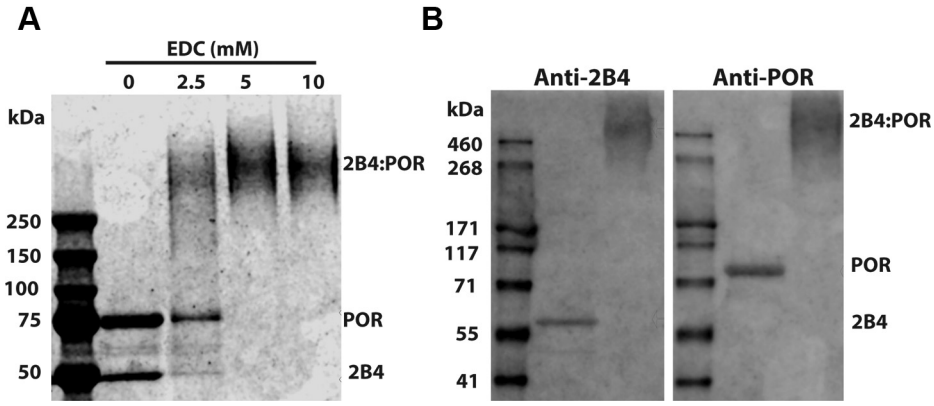


**Figure 3. Chemical crosslinking of the CYP2B4:POR complex in APols with EDC**. *A*, SDS-PAGE of the purified complex crosslinked with EDC at 0, 2.5, 5, and 10 mM. *B*, Western blotting against CYP2B4 and POR in crosslinked products. APol, amphipol; EDC, 1-ethyl-3-(3-dimethylaminopropyl)-carbodiimide; POR, NADPH-cytochrome P450 oxidoreductase.

### *Construction of a 3D model of the CYP2B4:POR complex in APols*

To construct a model for the multiunit CYP2B4:POR complex based on the 3D EM map, we fit the coordinates of CYP2B4 (PDB ID:1SUO) and POR (PDB ID: 1JA1) as rigid bodies into the 3D EM map. To facilitate the fitting process, the initial positions of the N-termini of CYP2B4 and POR were oriented toward the APol. No constraints were imposed during the fitting. As shown in Figure 6*A*, two molecules of CYP2B4 in blue were well fit into the 3D EM map with a correlation value of 0.65. Two molecules of POR in green were also fit into the density map with a correlation value of 0.54. However some EM densities remained unoccupied, which may suggest conformational flexibility of POR. A closer view of the interface between POR and CYP2B4 is shown in Figure 6*B*. The two N termini are faced in the same directions in the APol. With this orientation, the FMN domain of POR is positioned to the proximal side of the heme of CYP2B4. The distance between the heme Fe and N5 of FMN, $D_{Fe\text{-}N5}$, is approximately 53 Å. This architecture resembles the closed conformation that we observed in the cryoEM structure of CYP102A1 (24), as shown in Figure 6*C*. In this closed conformation of CYP102A1, the $D_{Fe\text{-}N5}$ is approximately 44 Å.

## Discussion

In this work, we presented an alternative to apolipoprotein A-1 and peptide-based nanodiscs for incorporating CYP2B4 and POR into membrane mimetics. As we have demonstrated (see Fig. 1), incubation of CYP2B4 and POR together with APols overnight at 4 °C, free of any detergents, spontaneously resulted in the incorporation of both proteins into APol nanoparticles. After further purification a homogenous tetrameric complex of CYP2B4:POR was obtained. The complex is fully functional in demethylating benzphetamine with activity comparable with the CYP2B4 and POR reconstituted in DLPC liposomes (see Table 1). This is in marked contrast to a prior attempt where individual CYP79A1, CYP71E1, or POR was incorporated into APols, but not the complex (19). The

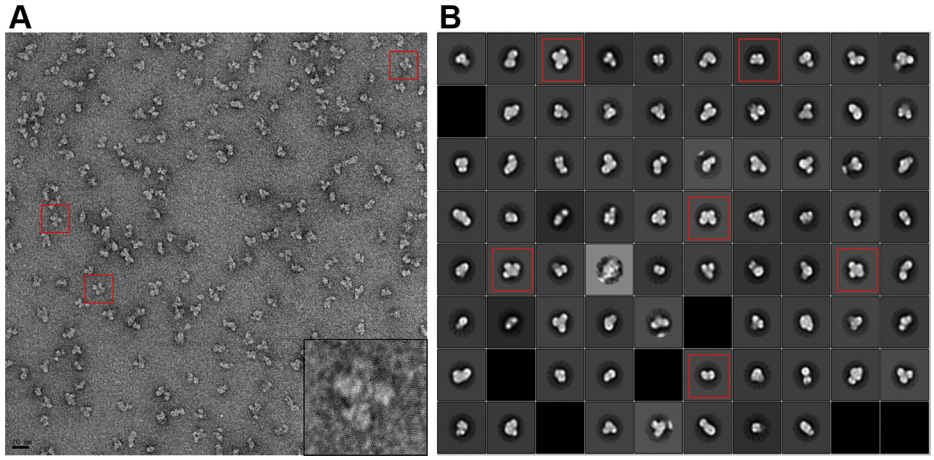


**Figure 4. Negative stain EM imaging and 2D classification of the CYP2B4:POR complex in APols**. The complex treated with GraFix was stained with 0.75% (w/v) uranyl formate prior to EM imaging. *A*, a representative micrograph of the complex. Single particles boxed in *red* indicate clear view of tetramers. An expanded view is shown in the inset. The *black* scale bar is 20 nm. *B*, reference-free 2D class averages of negative stain particles of the complex. A total of 10,766 single particles were aligned and classified into 80 classes. The 2D class averages boxed in *red* show a clear view of tetramer. APol, amphipol; EM, electron microscopy; POR, NADPH-cytochrome P450 oxidoreductase.

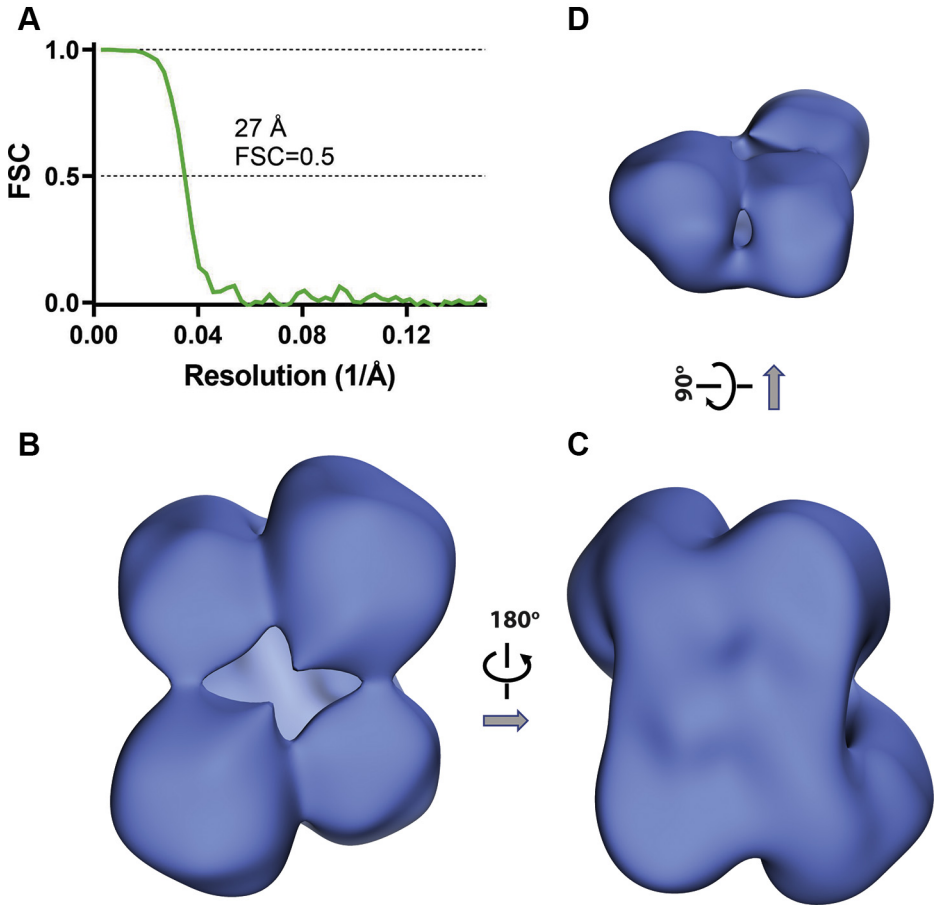


**Figure 5. Reconstructed 3D EM map for the CYP2B4:POR complex in APols**. The 3D EM map was reconstructed from ∼7000 particles with a C2 symmetry. *A*, Fourier shell correlation curve for the reconstruction. *B–D*, top, bottom, and side views of the reconstructed 3D EM maps respectively. APol, amphipol; EM, electron microscopy; POR, NADPH-cytochrome P450 oxidoreductase.

mixture of individual CYP79A1 and POR in APols exhibited only 1% of the catalytic activity compared with the CYP79A1 and POR reconstituted in DLPC liposomes. Our work represents the first successful incorporation of a functional complex of full-length CYP:POR complex in APol. Furthermore, the high homogeneity of our preparation is amendable to structural analysis by TEM. Small APol nanoparticles with a diameter of ∼50 Å (14) may be advantageous over large apolipoprotein A-1 or peptide-based nanodiscs (90–130 Å) (7, 9) such that the incorporated proteins of interest are the dominant feature in single particle analysis rather than the membrane mimetics.

Using negative stain EM, we were able to obtain a 3D EM map that reveals the architecture of the multiunit complex in membrane settings for the first time. The 3D EM map of the complex has a dimension of ∼150 Å and shows two pairs of densities (see Fig. 5), similar to what we reported for dimeric CYP102A1 (24, 25).

The 3D EM map of the complex bears two distinct differences from that of CYP102A1. One difference is the position of CYP2B4 relative to POR, and the other is the density at the bottom of the complex arising from the N termini and APols (see Fig. 5*C*). In CYP102A1, the two heme domains and two reductase domains are adjacent to each other. In particular, CYP102A1 is dimerized at the reductase domains providing stabilizing force for a functional dimer. This architecture allows a very efficient electron transfer from the reductase domain to the opposing heme domain. This is probably one of the main reasons why CYP102A1 is the most catalytically active P450 enzyme because the rate of electron transfer to the active site of P450s is often rate limiting (26). In contrast, the positions of CYP2B4 and POR are not adjacent to each other but across each other. This architecture leads to CYP2B4 adjacent to two POR and vice versa (see Fig. 6*A*). One of the interfaces between POR and CYP2B4 resembles that observed in CYP102A1 (see Fig. 6, *B* and *C*). The proximal side of CYP2B4 is faced to the FMN domain of POR. It is well established that POR interacts with the proximal side for electron transfer. In particular, several residues located in the C-helix and C/D loop regions such as Arg122, Arg126, Arg133, Phe135, and Met137 have been reported to be involved. For instance, mutations of the aforementioned residues to alanine decreased the ability to bind POR or cyt $b_5$ (27). In addition, results from solid state NMR studies of CYP2B4 complexed with the FMN-binding domain of POR in lipid bilayers showed Arg125 is important for effective electron transfer (9).

The orientation of CYP2B4 slightly rotates away from the FMN domain because of the presence of the connecting

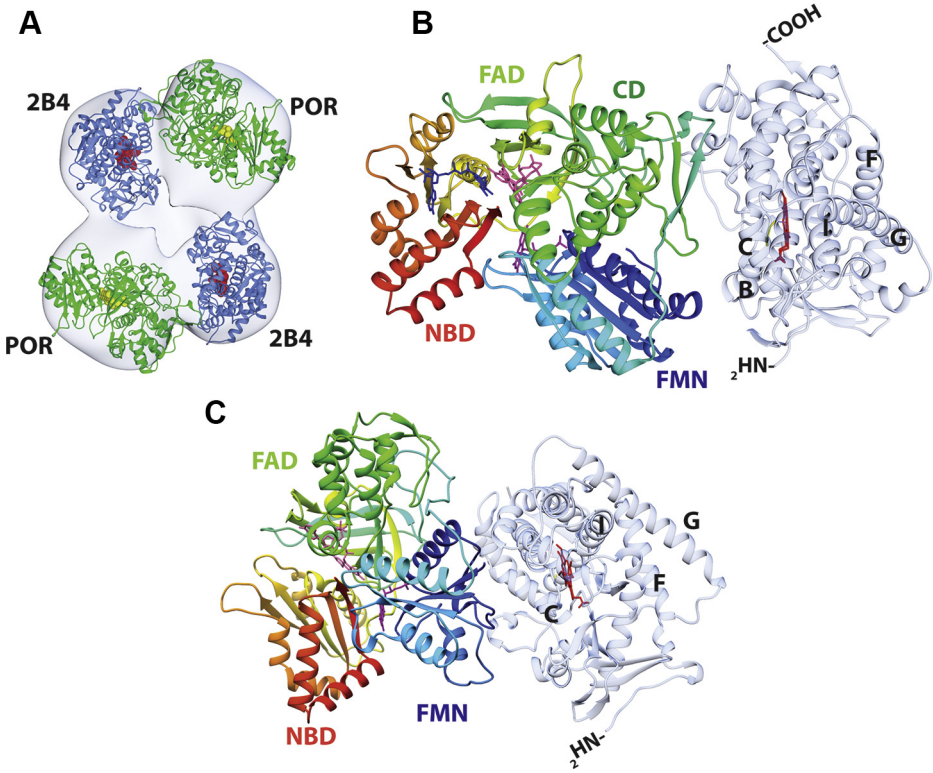


**Figure 6. Reconstructed 3D model of the CYP2B4:POR complex**. *A*, the crystal structures of CYP2B4 and POR were fit into the 3D EM map as rigid bodies. The backbones of CYP2B4 and POR are depicted as *blue* and *green ribbons* respectively. The heme and FMN cofactors are displayed as *red* and *yellow spheres* respectively. The 3D EM map is displayed as a transparent surface. *B*, a close view of the interface between CYP2B4 and POR. The backbone of CYP2B4 is displayed as transparent blue ribbons whereas the backbone of POR as rainbow ribbons from *blue* (N terminus) to *red* (C terminus). Cofactor heme, FMN, and FAD are displayed as *red*, *magenta*, and *pink* sticks, respectively. Helix B, C, F, G, and I of CYP2B4 are labeled. CD stands for the connecting domain of POR. *C*, closed conformation of CYP102A1 is displayed for comparison. The structure was derived from our prior EM map (EMDB ID:20785). The color scheme is identical to *Panel B*. EM, electron microscopy; POR, NADPH-cytochrome P450 oxidoreductase.

domain in POR which is absent from the reductase domain of CYP102A1. This rotation results in elongation of $D_{Fe\text{-}N5}$ from 43 to 53 Å, which undoubtedly reduces the rate of electron transfer from POR to CYP2B4. The turnover rates of mammalian P450s are generally two to three orders of magnitude slower than CYP102A1. It is also conceivable that large conformational changes may occur in POR during electron transfer to CYP2B4. As we reported (24), the FMN domain of CYP102A1 rotates out toward the proximal side of the heme to deliver the electrons. Based on the 3D model shown in Figure 6, we anticipate that this mechanism is retained in mammalian P450s where the FMN domain extends to an open conformation for electron transfer to CYP2B4. Despite the relatively long distance, this is achievable because of the highly flexible hinge region in POR. A full extension of the hinge observed in the open confirmation of POR increased the distance by ∼60 Å between closed and open conformation of POR (28).

The other difference is the orientations of POR and CYP2B4 where both N termini are faced in the same direction and embedded in APols. This is evidenced by the EM density at the bottom of the 3D EM map (see Fig. 5*C*). The architecture of the complex presented here seems to suggest that the N-termini provide anchoring forces. This is based on the lack of strong contacts between CYP2B4 and POR and also consistent with an early study demonstrating that the hydrophobic N-terminal segment of POR is involved in complexation with microsomal P450s and membranes (29). The anchoring force would enable CYP2B4 and POR to be positioned in the ER membranes, whereas the FMN domain undergoes transitions involving closed or open conformations for electron transfer. The motion of closed-to-open conformation should be similar to what was observed in CYP102A1 revealed by cryoEM (24). However, because of insufficient map resolution and deletion of N-terminal residues from the crystal structures of CYP2B4 and POR, we were unable to reveal the transmembrane anchoring segments critical for CYP2B4 and POR interactions. We envision that incorporation of multiunit complexes of P450s into APols would lead to further studies to investigate the interactions of P450 with POR, cyt $b_5$, or other P450 isozymes. In particular, structural study of these complexes using cryoEM may lead to high resolution structures capable of revealing the transmembrane domains and electron transfer complexes between P450 and its redox partners.

## Experimental procedures

### *Materials*

APol $A_{8\text{-}35}$ was purchased from Anatrace. NADPH, butylated hydroxytoluene, FAD, and benzphetamine were

purchased from Sigma Aldrich. DLPC was purchased from Doosan Serdary Research Laboratory. CO gas was purchased from Cryogenic Gas. Glutaraldehyde, uranyl formate, and EM grids were purchased from EMS. EDC was purchased from Thermo Fisher Scientific. Polyclonal POR antibody was purchased from Thermo Fisher Scientific, whereas polycolonal CYP2B4 antibody was from antibodies-online Inc. Ni-NTA resin was purchased from Qiagen.

### Overexpression and purification of full-length CYP2B4 and full-length POR

Rabbit WT CYP2B4 was overexpressed in *Escherichia coli* as the C-terminal His-tag protein and purified with an HisTrap HP column (GE HealthCare) as previously described (21, 25). Rat WT POR was overexpressed in *E. coli* and purified with a 2′,5′-ADP affinity column as previously reported (30). The concentration of CYP2B4 was determined using an extinction coefficient of $\Delta\varepsilon_{450-490nm}$ of 91 $mM^{-1}$ $cm^{-1}$ for the ferrous CO form of CYP2B4 (31), whereas the concentration of POR was determined using an extinction coefficient of 21 $mM^{-1}$ $cm^{-1}$ at 456 nm for the oxidized enzyme (32).

### Preparation and purification of the CYP2B4:POR complex in APols

Purified POR and C-terminal His-tag CYP2B4 (∼1–10 μM each) were incubated overnight with APol $A_{8-35}$ at a protein-to-APol ratio of 2:1 (w/w) in ∼6 ml of Buffer A (40 mM Hepes, pH 7.4, 15% (v/v) glycerol, 0.1 M NaCl, 50 μM butylated hydroxytoluene). To isolate the CYP2B4:POR complex, Ni-NTA resin was added to the incubation to bind the complex. The Ni-NTA resin was then recovered by centrifugation at 850*g*, washed with Buffer B (Buffer A + 10 mM imidazole), and finally eluted with Buffer C (Buffer A + 0.3 M imidazole). The eluted protein was concentrated to ∼10 μM and further purified by SEC in Buffer D (40 mM Hepes, pH 7.4, 0.1 M NaCl). The peak fractions were concentrated and stored on ice until use.

### Determination of stoichiometry of the CYP2B4:POR complex in APol

The stoichiometry of the complex was determined by quantifying both proteins and co-factors. The amount of protein was quantified by gel densitometry following SDS-PAGE using Image Studio software (Ver. 5.2, LI-COR). The heme of CYP2B4 was quantified by the hemochromogen method as described (33), whereas the FAD of POR was quantified by HPLC as we previously reported (34).

### Determination of the molecular weight of the CYP2B4:POR complex in APol by SEC-MALS

The molecular weight $M_w$ of the complex was determined by SEC-MALS on a Bio-Rad NGC liquid chromatography system equipped with a miniDawn TREOS MALS detector and an Optilab TrEX differential refractive index detector, as we previously described (25). Briefly, an aliquot (∼100 μl) of the complex at ∼10 μM was loaded onto a SEC column (WTC-MP050S5, 7.8 × 300 mm, 5 μm, Wyatt Technology) and separated at a flow rate of 0.5 ml/min in Buffer D containing 0.05% (w/v) sodium azide. The $M_w$ value was determined from the Raleigh ratio calculated by measuring the static light scattering and corresponding protein concentration using ASTRA VI software (Wyatt Technology). The SEC-MALS system was calibrated with bovine serum albumin.

### Catalytic activity and coupling of the CYP2B4:POR complex in APol

To evaluate the effects of APol on the catalysis of CYP2B4, we determined the rates of both NADPH consumption and product formation, in comparison with conventionally reconstituted CYP2B4 and POR in DLPC liposomes. Equal molar ratios of CYP2B4 and POR were reconstituted in DLPC liposomes as we previously reported (21). The rate of the NADPH consumption was determined at 37 °C in Buffer D containing 0.05 μM CYP2B4, 1 mM benzphetamine, and 0.24 mM NADPH. The reaction was initiated by adding NADPH and monitored at 340 nm for 3 min. The NADPH consumption rate was calculated from the slope using the NADPH extinction coefficient of 6.4 $mM^{-1}$ $cm^{-1}$. All experiments were performed at least in duplicate. The rate of product formation was determined from the aforementioned samples by quantifying the amount of norbenzphetamine using LC-MS/MS as we previously reported (34).

### Chemical crosslinking of the CYP2B4:POR complex in APol

To stabilize the complex, the purified complex (∼5 μM) was crosslinked at various EDC concentrations (0–10 mM) at 25 °C for 2 h. The crosslink reaction was terminated by adding hydroxylamine to 10 mM. The crosslinked samples were then denatured and subjected to SDS-PAGE and Western blotting analysis. For negative stain EM, the complex was crosslinked with glutaraldehyde using GraFix as described (23). In brief, gradients of sucrose (10–30% w/v) and glutaraldehyde (0–0.5% v/v) were prepared using a gradient master (Model 108, BioComp Instruments Inc). Aliquots of the SEC-purified CYP2B4:POR complex in APol were loaded on top of the light sucrose solution and centrifuged at 200,000*g* for 15 to 17 h. Crosslinked protein complex was fractionated using a BioComp GradiFrac Fractionator. The central fraction was subsequently used for negative stain EM as described below.

### Negative stain EM data acquisition and image processing

The central fraction from the GraFix experiment was applied to carbon-coated copper grids and stained with ∼0.75% (w/v) uranyl formate. EM data were collected on a G2 Spirit TEM (FEI Tecnai T12) operated at 120 kV. A total of ∼200 micrograph images were recorded at 50,000× nominal magnification using a CCD camera (Gatan). The micrographs were processed using Relion 3.0.8 software, including particle picking, 2D classification, *ab initio* reconstruction, and refinement (35). After few rounds of 2D classification to remove false positive particles, a total of 10,766 particles were used to build the initial model with a C1 symmetry. After 3D

classification, a subset of ~7000 particle in the initial model exhibited nearly a C2 symmetry and were further refined with the C2 symmetry to construct the final 3D EM map at 27 Å.

### *Construction of a 3D model of the CYP2B4:POR complex*

The 3D model of tetrameric complex of CYP2B4:POR was constructed by docking the crystal structures of CYP2B4 and POR as rigid bodies into the 3D EM map using the fitmap function of Chimera (36). The coordinates of CYP2B4 (PDB ID: 1SUO) and POR (PDB ID: 1JA1) were obtained from the Protein Data Bank. It is noteworthy that the coordinates of CYP2B4 and POR did not contain the N-terminal transmembrane anchors. The initial positions of truncated CYP2B4 and POR were oriented such that the N termini of both proteins were faced to the APol to facilitate the fitting process. Rigid-body fitting was then performed without any constraints. The final model was selected based on map correlation as we previously described (24).

## Data availability

All associated data are contained within the article or available upon request to the authors.

*Supporting information*—This article contains supporting information.

*Acknowledgments*—We are grateful for technical assistance from the staff scientists, Drs. Min Su, Amy Bondy, and Laura Koepping, at the Microscopy Core Facilities of Life Sciences Institute to acquire EM images. This work was supported by grants from the National Institutes of Health (GM077430 and ES030791). The content is solely the responsibility of the authors and does not necessarily represent the official views of the National Institutes of Health.

*Author contributions*—Y. O. and H. Z. conceived and supervised the study; S. C., Z. B., and H. Z. performed the experiments; S. C., Z. B., and H. Z. drafted the manuscript. All authors edited and reviewed the manuscript.

*Conflict of interest*—The authors declare that they have no conflicts of interest with the contents of this article.

*Abbreviations*—The abbreviations used are: APol, amphipol; CYP, cytochrome P450; DLPC, 1,2-dilauroyl-sn-glycero-3-phosphocholine; EDC, 1-ethyl-3-(3-dimethylaminopropyl)-carbodiimide; EM, electron microscopy; FAD, flavin adenine dinucleotide; POR, NADPH-cytochrome P450 oxidoreductase; SEC, size-exclusion chromatography; SEC-MALS, SEC-multiangle light scattering.

## References

1. Guengerich, F. P. (1995) Human cytochrome P450 enzymes. In: de Montellano, P. R., ed. *Cytochrome P450: Structure, Mechanism, and Biochemistry*, Plenum, New York, NY: 473–535
2. Martinez, S. E., Shi, J., Zhu, H. J., Perez Jimenez, T. E., Zhu, Z., and Court, M. H. (2019) Absolute quantitation of drug-metabolizing cytochrome P450 enzymes and accessory proteins in dog liver microsomes using label-free standard-free analysis reveals interbreed variability. *Drug Metab. Dispos.* **47**, 1314–1324
3. Peterson, J. A., Ebel, R. E., O'Keeffe, D. H., Matsubara, T., and Estabrook, R. W. (1976) Temperature dependence of cytochrome P-450 reduction. A model for NADPH-cytochrome P-450 reductase:cytochrome P-450 interaction. *J. Biol. Chem.* **251**, 4010–4016
4. Omura, T., and Sato, R. (1962) A new cytochrome in liver microsomes. *J. Biol. Chem.* **237**, 1375–1376
5. Lu, A. Y., Junk, K. W., and Coon, M. J. (1969) Resolution of the cytochrome P-450-containing omega-hydroxylation system of liver microsomes into three components. *J. Biol. Chem.* **244**, 3714–3721
6. Denisov, I. G., and Sligar, S. G. (2011) Cytochromes P450 in nanodiscs. *Biochim. Biophys. Acta* **1814**, 223–229
7. Denisov, I. G., Grinkova, Y. V., Lazarides, A. A., and Sligar, S. G. (2004) Directed self-assembly of monodisperse phospholipid bilayer Nanodiscs with controlled size. *J. Am. Chem. Soc.* **126**, 3477–3487
8. Zhang, M., Huang, R., Ackermann, R., Im, S. C., Waskell, L., Schwendeman, A., and Ramamoorthy, A. (2016) Reconstitution of the Cyt$b_5$-CytP450 complex in nanodiscs for structural studies using NMR spectroscopy. *Angew. Chem. Int. Ed. Engl.* **55**, 4497–4499
9. Prade, E., Mahajan, M., Im, S. C., Zhang, M., Gentry, K. A., Anantharamaiah, G. M., Waskell, L., and Ramamoorthy, A. (2018) A minimal functional complex of cytochrome P450 and FBD of cytochrome P450 reductase in Nanodiscs. *Angew. Chem. Int. Ed. Engl.* **57**, 8458–8462
10. Bayburt, T. H., and Sligar, S. G. (2002) Single-molecule height measurements on microsomal cytochrome P450 in nanometer-scale phospholipid bilayer disks. *Proc. Natl. Acad. Sci. U. S. A* **99**, 6725–6730
11. Mahajan, M., Ravula, T., Prade, E., Anantharamaiah, G. M., and Ramamoorthy, A. (2019) Probing membrane enhanced protein-protein interactions in a minimal redox complex of cytochrome-P450 and P450-reductase. *Chem. Commun. (Camb.)* **55**, 5777–5780
12. Mukherjee, G., Nandekar, P. P., and Wade, R. C. (2021) An electron transfer competent structural ensemble of membrane-bound cytochrome P450 1A1 and cytochrome P450 oxidoreductase. *Commun. Biol.* **4**, 55
13. Sellner, M., Fischer, A., Don, C. G., and Smiesko, M. (2021) Conformational landscape of cytochrome P450 reductase interactions. *Int. J. Mol. Sci.* **22**, 1023
14. Gohon, Y., Giusti, F., Prata, C., Charvolin, D., Timmins, P., Ebel, C., Tribet, C., and Popot, J. L. (2006) Well-defined nanoparticles formed by hydrophobic assembly of a short and polydisperse random terpolymer, amphipol $A_{8\text{-}35}$. *Langmuir* **22**, 1281–1290
15. Popot, J. L. (2010) Amphipols, nanodiscs, and fluorinated surfactants: Three nonconventional approaches to studying membrane proteins in aqueous solutions. *Annu. Rev. Biochem.* **79**, 737–775
16. Tribet, C., Audebert, R., and Popot, J. L. (1996) Amphipols: Polymers that keep membrane proteins soluble in aqueous solutions. *Proc. Natl. Acad. Sci. U. S. A.* **93**, 15047–15050
17. Duan, J., Li, Z., Li, J., Hulse, R. E., Santa-Cruz, A., Valinsky, W. C., Abiria, S. A., Krapivinsky, G., Zhang, J., and Clapham, D. E. (2018) Structure of the mammalian TRPM7, a magnesium channel required during embryonic development. *Proc. Natl. Acad. Sci. U. S. A.* **115**, E8201–E8210
18. Hulse, R. E., Li, Z., Huang, R. K., Zhang, J., and Clapham, D. E. (2018) Cryo-EM structure of the polycystin 2-l1 ion channel. *Elife* **7**, e36931
19. Laursen, T., Naur, P., and Moller, B. L. (2013) Amphipol trapping of a functional CYP system. *Biotechnol. Appl. Biochem.* **60**, 119–127
20. Gruenke, L. D., Konopka, K., Cadieu, M., and Waskell, L. (1995) The stoichiometry of the cytochrome P-450-catalyzed metabolism of methoxyflurane and benzphetamine in the presence and absence of cytochrome $b_5$. *J. Biol. Chem.* **270**, 24707–24718
21. Zhang, H., Im, S. C., and Waskell, L. (2007) Cytochrome $b_5$ increases the rate of product formation by cytochrome P450 2B4 and competes with cytochrome P450 reductase for a binding site on cytochrome P450 2B4. *J. Biol. Chem.* **282**, 29766–29776
22. Griffith, I. P. (1972) The effect of cross-links on the mobility of proteins in dodecyl sulphate-polyacrylamide gels. *Biochem. J.* **126**, 553–560
23. Kastner, B., Fischer, N., Golas, M. M., Sander, B., Dube, P., Boehringer, D., Hartmuth, K., Deckert, J., Hauer, F., Wolf, E., Uchtenhagen, H., Urlaub, H., Herzog, F., Peters, J. M., Poerschke, D., *et al.* (2008) GraFix:

Sample preparation for single-particle electron cryomicroscopy. *Nat. Methods* **5**, 53–55
24. Su, M., Chakraborty, S., Osawa, Y., and Zhang, H. (2020) Cryo-EM reveals the architecture of the dimeric cytochrome P450 CYP102A1 enzyme and conformational changes required for redox partner recognition. *J. Biol. Chem.* **295**, 1637–1645
25. Zhang, H., Yokom, A. L., Cheng, S., Su, M., Hollenberg, P. F., Southworth, D. R., and Osawa, Y. (2018) The full-length cytochrome P450 enzyme CYP102A1 dimerizes at its reductase domains and has flexible heme domains for efficient catalysis. *J. Biol. Chem.* **293**, 7727–7736
26. Pearl, N. M., Wilcoxen, J., Im, S., Kunz, R., Darty, J., Britt, R. D., Ragsdale, S. W., and Waskell, L. (2016) Protonation of the hydroperoxo intermediate of cytochrome P450 2B4 is slower in the presence of cytochrome P450 reductase than in the presence of cytochrome $b_5$. *Biochemistry* **55**, 6558–6567
27. Bridges, A., Gruenke, L., Chang, Y. T., Vakser, I. A., Loew, G., and Waskell, L. (1998) Identification of the binding site on cytochrome P450 2B4 for cytochrome $b_5$ and cytochrome P450 reductase. *J. Biol. Chem.* **273**, 17036–17049
28. Hamdane, D., Xia, C., Im, S. C., Zhang, H., Kim, J. J., and Waskell, L. (2009) Structure and function of an NADPH-cytochrome P450 oxidoreductase in an open conformation capable of reducing cytochrome P450. *J. Biol. Chem.* **284**, 11374–11384
29. Black, S. D., French, J. S., Williams, C. H., Jr., and Coon, M. J. (1979) Role of a hydrophobic polypeptide in the N-terminal region of NADPH-cytochrome P-450 reductase in complex formation with P-450LM. *Biochem. Biophys. Res. Commun.* **91**, 1528–1535
30. Shen, A. L., Porter, T. D., Wilson, T. E., and Kasper, C. B. (1989) Structural analysis of the FMN binding domain of NADPH-cytochrome P-450 oxidoreductase by site-directed mutagenesis. *J. Biol. Chem.* **264**, 7584–7589
31. Omura, T., and Sato, R. (1964) The carbon monoxide-binding pigment of liver microsomes. I. Evidence for its hemoprotein nature. *J. Biol. Chem.* **239**, 2370–2378
32. Vermilion, J. L., and Coon, M. J. (1978) Purified liver microsomal NADPH-cytochrome P-450 reductase. Spectral characterization of oxidation-reduction states. *J. Biol. Chem.* **253**, 2694–2704
33. Paul, K. G., Theorell, H., and Akeson, A. (1953) The molar light absorption of pyridine ferroprotoporphyrin (Pyridine haemochromogen). *Acta Chem. Sacnd.* **7**, 1284–1287
34. Zhang, H., Gruenke, L., Arscott, D., Shen, A., Kasper, C., Harris, D. L., Glavanovich, M., Johnson, R., and Waskell, L. (2003) Determination of the rate of reduction of oxyferrous cytochrome P450 2B4 by 5-deazariboflavin adenine dinucleotide T491V cytochrome P450 reductase. *Biochemistry* **42**, 11594–11603
35. Scheres, S. H. (2012) RELION: Implementation of a Bayesian approach to cryo-EM structure determination. *J. Struct. Biol.* **180**, 519–530
36. Pettersen, E. F., Goddard, T. D., Huang, C. C., Couch, G. S., Greenblatt, D. M., Meng, E. C., and Ferrin, T. E. (2004) UCSF Chimera–a visualization system for exploratory research and analysis. *J. Comput. Chem.* **25**, 1605–1612